CAPILLARY END EFFECTS AND GAS PRODUCTION FROM LOW PERMEABILITY FORMATIONS

Richard Christiansen, Colorado School of Mines, Carolina Mayoral, Carlos Pereira, Questa Engineering

This paper was prepared for presentation at the International Symposium of the Society of Core Analysts held in Toronto, Canada, 21-15 August 2005

ABSTRACT

Effects on gas productivity of leakoff during fracturing and imbibition of water during the productive life of gas wells in low permeability formations are described with results of 1D and 3D reservoir models that allow for capillary end effects – water blocks. Results show that loss of gas productivity is sensitive to capillary pressure and relative permeability relationships, in addition to pressure drawdown and permeability. Water blocks produce a large pressure drop at the fracture face. The fracture-face pressure drop will vary from 100 to 1000 psi, depending on rock-fluid properties. Cumulative lost production may be as much as 30%.

INTRODUCTION

Liquid water (or even liquid hydrocarbon) can accumulate in the bottom of a gas well when the gas flow rate falls below a critical value. This critical flow rate can be estimated with an expression proposed by Turner *et al*.[1] and later modified by Coleman *et al*.[2] According to those authors, the critical flow rate is the product of the cross-sectional area of the tubing through which the gas is flowing and the critical velocity:

$$v_c = M\left[\frac{(\rho_l - \rho_g)\sigma_{gl}}{\rho_g^{\,2}}\right]^{1/4} \qquad (1)$$

in which M is between 0.57 and 0.68 for critical velocity in units of ft/sec, liquid density ρ_l and the gas density ρ_g in units of g/cm^3, and gas-liquid interfacial tension σ_{lg} in units of dyne/cm. For conditions typical of many mature gas wells in the US, the critical flow rate is between 300 and 600 Mscf/day for 2 3/8-inch tubing (which has an ID of 2 inches). Frequently, the tubing ends above the top perforation from the casing to gas-bearing formations. With casing IDs of 4 or more inches, the critical flow rate in the casing is four or more times the tubing critical rate. More than 90% of US gas wells produce below their critical flow rates. The water that accumulates in these wells may be liquid water from an aquifer or a gas bearing formation, or it may be vaporized water that condenses as it travels up the well and then falls back to the bottom of the well. Wells with condensed water are a focus of this paper.

Condensed water that accumulates at the bottom of a gas well decreases productivity of the well in two ways. First, it increases the bottom-hole pressure, which decreases productivity. Second, water that imbibes from the well into the producing formation in the near-well region can block gas flow by reducing relative permeability of gas. If the well has been hydraulically fractured, the liquid water at the bottom of the well can enter the fracture and saturate the near-fracture region of the producing formation, also decreasing productivity. In 1979, Holditch[3] examined the impact of water blocks that form during stimulation on productivity of gas wells. He concluded that gas production can be severely impaired if the drawdown pressure does not exceed the capillary pressure and the water mobility is low. Similar conclusions were reached in recent studies[4,5]. These studies directed attention to evaporation of water from the near-fracture region.

For this paper, we investigated the effect of water blocks on gas productivity using a combination of in-house and commercial reservoir simulators. We used rock and fluid properties that are common to gas reservoirs in the Rocky Mountains. The effects of variations in the rock-fluid properties have been studied extensively.

SIGNIFICANCE OF CAPILLARY-DRIVEN FLOW

It can be shown that the fractional flow of water for a one-dimensional gas-water displacement is as follows[Chapter 3 of Reference 6]:

$$f_w = \frac{1 + \dfrac{k k_{rg} A}{q \mu_g}\left(\dfrac{\partial P_c}{\partial x} - \Delta\rho g \sin\theta\right)}{1 + \dfrac{\mu_w}{k_{rw}}\dfrac{k_{rg}}{\mu_g}} \tag{2}$$

with $P_c = P_g - P_w$ and $\Delta\rho = \rho_w - \rho_g$. As expressed in the numerator of the above equation, the water fractional flow is the sum of three parts: a mobility term, a capillary pressure term, and a gravity term. The driving force for the capillary pressure term is the gradient of the capillary pressure, which can be obtained from the capillary pressure relationship for a specific formation. For this work, we used the Bentsen-Anli expression for representing the capillary pressure relationship:

$$P_c = P_{ct} - P_{cs} \ln\left[\frac{S_w - S_{wi}}{1 - S_{wi}}\right] \tag{3}$$

Equation 3 is often used for primary drainage. For much of the saturation domain of this paper, imbibition is important. Nevertheless, Eq. 3 was chosen because we have no imbibition data for low permeability formations. Proceeding from Eq. 3, the gradient of capillary pressure is as follows:

$$\frac{\partial P_c}{\partial x} = -P_{cs}\left[\frac{1-S_{wi}}{S_w - S_{wi}}\right]\frac{\partial S_w}{\partial x} \tag{4}$$

Thus, the magnitude of the capillary-driven flow depends on P_{cs}, water saturation, and the saturation gradient. The following correlation for P_{cs} is qualitatively consistent with data from Newsham *et al*.[7] for the Bossier sand:

$$P_{cs} = 150\, k^{-0.5} \tag{5}$$

For permeability of 0.01 md, Eq. 5 gives P_{cs} equal to 1500 psi. The correlation of Eq. 5 for P_{cs} is similar in form to correlations proposed by Thomas *et al*.[8} and other investigators[9] for the threshold pressure of low permeability sandstones. Confining stress was absent for the data correlated with Eq. 5. As a result, Eq. 5 should underestimate P_{cs} at reservoir stresses for most low permeability rocks because their permeabilities can drop by 20 times as stress increases to typical reservoir levels[10]. If stress sensitivity of k is known, then values obtained from Eq. 5 can be adjusted approximately using the square root of the ratio of permeabilities from the unstressed to the stressed condition.

The significance of capillary-driven flow for low permeability formations can be assessed using Eq. 2. Using typical values for flow rates, dimensions of hydraulic fractures, permeabilities, gas viscosities, with P_{cs} from Eq. 5, and with saturation gradients between 0.1 and 1.0 per foot, the dimensionless capillary term of Eq. 2 falls between 1 and 20. Thus, for horizontal formations, the capillary-driven portion of fractional flow equals or exceeds the mobility term.

APPROACH

In-House Simulator

The in-house simulator represents one-dimensional immiscible and incompressible displacements. It uses a modified IMPES algorithm. It was originally developed for simulating capillary end effects for laboratory-scale displacements. To simulate end effects, capillary pressure is set to zero in the outlet node of the finite difference model. See Chapter 7 of Reference 6 for details. The model proved quite useful for the present study. It provided for imbibition and retention of water for the system consisting of low permeability rock that produces gas to a water-saturated fracture as shown in Figure 1. And the model allows for rapid adjustment of capillary pressure and relative permeability behavior.

We used the in-house simulator for two purposes: to estimate the extent of invasion of water during hydraulic fracturing into a largely gas-saturated rock sample, and to study the invasion of water during gas production. For modeling water invasion during fracturing, the initial saturation of water in the sample was set slightly above the irreducible water saturation S_{wi}. For modeling water invasion during gas production, the

initial water saturation was uniform for most of the sample length except near the outlet end where a short zone of high water saturation was specified to represent the zone invaded during fracturing. Furthermore, we assume that water remains in the fracture during the gas production cycle. For many gas wells, this is a good assumption because gas flow rates are often insufficient to blow all water up the casing to the end of the tubing in the well.

The in-house simulator uses modified Brooks-Corey relations for relative permeabilities of the gas and water:

$$k_{rg} = k_{rg,\max}\left(\frac{S_g - S_{gc}}{1 - S_{wi} - S_{gc}}\right)^{ng} \qquad k_{rw} = k_{rw,\max}\left(\frac{S_w - S_{wi}}{1 - S_{wi} - S_{gc}}\right)^{nw} \qquad (6)$$

To represent capillary pressure, the simulator uses the Bentsen-Anli expression (Eq. 3).

Commercial Simulator

A commercial reservoir simulator (Eclipse 100) was used to evaluate the effects of near-well and near-fracture water saturation on gas reservoir performance. As for most black-oil simulators, this simulator does not allow vaporization of water. Therefore, this process is often neglected in studies of gas reservoirs. Here, we fooled the simulator into including vaporization of water by entering water data in a vaporization table in place of oil data – the simulator allows for vaporization of the oil component. This approach avoids the complexity of the compositional simulation and reduces the time required for the simulation by having fewer unknowns. Properties of the gas and water were estimated with correlations from McCain[11] and Reid *et al*.[12] for a reservoir temperature of 160˚F and initial pressure of 3500 psi.

Radial (Base Case k = 0.5 md) and Cartesian (Base Case k = 0.05 md) coordinate models were used to investigate the effect of liquid loading on reservoir productivity in non-fractured and fractured formations, respectively. Reservoir and fluid properties used in these conceptual models are similar to some Rocky Mountain gas reservoirs.

The drainage area of the radial model is 80 acres. The model has 11 divisions in the r-direction, and 3 layers (each 10 feet thick) in the vertical direction. The radial width of the divisions varied from under 1 foot for the divisions nearest the well to more than 500 feet in the outer-most division: 0.4 0.8 3 6 9 16 32 64 128 256 538 (all in feet). The model has one injector and one producer both located on the central axis of the grid. The producer well was completed in all three layers; and the injector was completed in the upper two layers.

The Cartesian model has an area of 80 acres divided into 1479 cells: 29 by 17 divisions in the xy-horizontal plane (1941 feet by 1795 feet), and 3 layers (each 10 feet thick) in the vertical direction.

x-divisions (ft): 173 7*100 50 20 10 8 6 3 1 3 6 8 10 20 50 7*100 173
y-divisions (ft): 5*160 60 25 10 5 10 25 60 5*160

To represent a hydraulic fracture, a high permeability region (100 md) was defined by x-row 15 (of 29) and y-rows 6 through 12 (of 17) in all three layers. The high permeability zone was 1 foot thick, 195 feet from end to end, and 30 feet tall. The product of permeability and thickness for this fracture (100 md ft) is in the ballpark of what is expected for actual fractures that are usually less than 0.5 inch thick. The producer well was completed in the top layer in the middle division along the length of the fracture. See Figure 2. An injector well was located at each end of the fracture region.

A typical simulation was as follows. The producing well was allowed to deliver gas without interruption with a bottom-hole pressure of 400 psi until the production rate fell to about 300 MCF/day. At that point, the production well was temporarily shut (3 to 4 days) while the injector wells were activated with a constant water injection rate. After that, the injectors were shut and the producer was re-opened. This procedure was intended to represent temporary shut-in of actual producing wells, during which time water could imbibe from the well back into the formation. Many variations on this simulation scheme were implemented. In some cases, water was injected continually at a low rate after gas production fell to about 300 MCF/day. In many cases, the water injection process was repeated on a two-month cycle. In some cases, the repeat period was one year. During the injection period, volume of water injected varied from 1 to 20 Bbl/day.

RESULTS

In-House Simulator

The in-house model was used first to estimate the depth of penetration of water during hydraulic fracturing with a 2000 psi pressure drop pushing water into 3 feet of low permeability rock. Effects of dissolved polymers on invasion of the water were ignored because of uncertainty about the transport of polymers in very low permeability rock. Extent of invasion of water is shown for k = 0.01 md in Figure 3. The extent of invasion in Figure 3 is similar to that estimated from logs for invasion during drilling in the Rulison Field of Western Colorado. This gives some confidence in the predictions of the model.

Next, the in-house model was used to investigate the effect of water invasion on production of gas after hydraulic fracturing is completed. To simplify this modeling process, the initial profile of water saturation was specified with a step function near the fracture. Adjacent to the fracture, the water saturation was 1- S_{gc}. Away from the fracture, the water saturation equaled S_{wi}. The width of the step was varied. In the paragraphs below, results of a Base Case simulation are first presented, then results for variations from the Base Case are given. For all of these cases, the length of the simulated formation is 100 feet. The pressure drop for all cases is the difference in pressure from the left end of the model to the fracture face in Figure 1.

Results for the Base Case are shown in Figures 4 to 6 for parameters listed in the caption of Figure 4. Figure 4 shows evolution of the saturation profile over 50 days from the initially imposed step function profile. The depth of water invasion slowly increases with time as water in the fracture imbibes into the low permeability rock. During that 50-day period, the pressure profile evolves as shown in Figure 5. Initially, there is a very large pressure drop near the fracture caused by the water block that invaded during the stimulation process. Over time, the near-fracture pressure drop falls to a lower value, but it remains significantly large. Zero on the scale for the pressure profile is a reference pressure and not a true zero, because the fluids are incompressible in this model. The flow-rate ratio of Figure 6 is defined as the gas flow rate obtained from the simulation divided by the gas flow rate that would have occurred in the absence of water accumulation near the fracture. The flow-rate ratio for the Base Case rises to a maximum value of about 0.7 after five days of gas production. The increase in flow-rate ratio corresponds to healing of the initial step function saturation profile. The flow-rate ratio declines at a very slow rate from the maximum value as invasion of water proceeds into the gas producing formation.

Figure 6 also shows the flow-rate ratio for two variations from the Base Case, having pressure drops of 500 and 250 psi across the 100-ft length of the model. Clearly, the difference between reservoir pressure and bottom-hole pressure is an important factor for predicting the significance of water blocks on gas production. Many mature and even some more recently identified gas reservoirs have low reservoir pressures. Water blocks can significantly impair production of gas from these reservoirs unless steps are taken to minimize the blocks. Some operators have added methanol to the water used in fracturing.

Figure 7 shows a third variation from the Base Case in which the shape of the gas relative permeability relationship was altered by changing the exponent *ng* from 2 to 4. This change reduces gas relative permeability for the entire saturation range. For this variation, time to recovery of maximum gas production rate is about 10 days. And the maximum flow-rate ratio is 0.5, which is significantly less than the Base Case.

Effects of increasing P_{cs} from the Base Case value of 500 psi are shown in Figure 8. Increasing P_{cs} leads to three changes: it reduces the time to reach maximum gas flow rate, it reduces the maximum flow-rate ratio, and it increases the rate of decline in gas flow rate after the maximum is reached. The time to reach maximum gas flow rate decreases because the rate of capillary-driven flow increases with higher P_{cs}. At the same time, higher P_{cs} pulls liquid into the formation faster, which leads to reduced maximum flow rate and more rapid decline in production.

Figure 9 shows the effect of changing the depth of invasion (Step Width) from the Base Case value of 1.25 ft. Production rate recovery is faster with less invasion and much slower with more invasion.

Commercial Simulator

Most of the results summarized here are for the Radial model. With this model, we evaluated effects of absolute permeability, vertical–horizontal permeability ratio, modified Brooks and Corey exponents and end points of relative permeability functions, capillary pressure, and the water vaporization effect.

The results indicate the effect of the absolute permeability, the vertical-horizontal permeability ratio, the shape of the relative permeability curves, and the vaporized water have an important effect on the gas well performance when liquid loading problems is present.

According to simulation results, the absolute permeability has the most significant effect on the gas well production. Table 1 shows the loss in cumulative gas production over a 15-year production period for three values of permeability. Cumulative loss is greatest for the lowest permeability. Low permeability formations require higher drawdown pressure to remove the water block. In our simulations, the bottom-hole pressure was the same for all permeabilities.

The curvature of the relative permeability curves had the second most important impact in the gas well performance. The results in Table 2 show increase loss of cumulative gas production as the water and gas exponents of the Brooks-Corey expressions for relative permeability increase. When the modified Brooks and Corey exponents increase the relative permeability of the water and gas decrease. As a result, the near wellbore region cannot be cleaned up and the gas production decreases. The end-points of the relative permeability expressions had very little effect on loss of gas production.

As expected, vaporization has a positive effect on gas production because it provides another mechanism for removal of water blocks. Including vaporization decreased the lost gas production from 24% to 20% for the base case Radial model.

Results from the Cartesian model do not show as much impact of water blocks on gas recovery. However, that may be a consequence of grid-size distribution or other details of the model. We are currently exploring these issues.

CONCLUSIONS

1. Results of in-house and commercial simulators show that water blocks reduce rate of gas production, especially from low permeability formations.
2. Magnitude of the reduced rate of production caused by water blocks depends on pressure drawdown, formation permeability, capillary pressures, and relative permeaiblities.
3. Evaporation of water reduces the effect of water blocks.
4. Capillary-driven flow is very significant in low permeability formations.

REFERENCES

1. Turner, R. G., Hubbard, M. G., and Dukler, A. E.: "Analysis and Prediction of Minimum Flow Rate for the Continuous Removal of Liquids from Gas Wells," *J. Pet. Tech*. (November 1969) 1475-1482.
2. Coleman, S. B., Clay, H. B., McCurdy, D. G., and Norris, H. L., III: "A New Look at Predicting Gas-Well Load-Up," *J. Pet. Tech.* (March 1991) 329-333.
3. Holditch, S. A.: "Factors Affecting Water blocking and Gas flow from Hydraulically Fractured Gas Wells," J. Pet. Tech. (December 1979) 1515-1524.
4. Parekh, B., and Sharma, M. M.: "Cleanup of Water Blocks in Depleted Low-Permeability Reservoirs," Paper 89837 presented at the 2004 SPE Annual Technical Conference and Exhibition, Houston, TX, September 26-29.
5. Mahadevan, J., Sharma, M. M., and Yortsos, Y. C.: "Evaporative Clean-Up of Water-Blocks in Gas Wells," Paper 94215 presented at the 2005 SPE Production and Operations Symposium, Oklahoma City, OK, April 17-19.
6. Christiansen, R. L.: *Two-Phase Flow through Porous Media*, KNQ Engineering (2001).
7. Newsham, K. E., Rushing, J. A., and Lasswell, P. M.: "Use of Vapor Desorption Data to Characterize High Capillary Pressures in a Basin-Centered Gas Accumulation with Ultra-Low Connate Water Saturations," Paper 84596 presented at the 2003 SPE Annual technical Conference and Exhibition, Denver, CO, October 5-8.
8. Thomas, L. K., Katz, D. L., and Tek, M. R.: "Threshold Pressure Phenomena in Porous Media," *Soc. Pet. Eng. J*. (June 1968) 174-184. Also in *Trans*., AIME (1968) **243**.
9. Smith, J. D., Chatzis, I., and Ioannidis, M. A.: "A New Technique for Measuring the Breakthrough Capillary Pressure," Paper 2002-40 presented at the 2002 International Symposium of the Society of Core Analysts, Monterey, CA, September 22-25.
10. Jones, F. O., and Owens, W. W.: "A Laboratory Study of Low-Permeability Gas Sands," J. Pet. Tech. (September 1980) 1631-1640. Also in *Trans*., AIME (1980) **269**.
11. McCain, W. D., Jr.: *The Properties of Petroleum Fluids*, Second Edition, PennWell Books, Tulsa, OK (1990) p. 528.
12. Reid, R. C., Prausnitz, J. M., and Poling, B. E.: *The Properties of Gases & Liquids*, Fourth Edition, McGraw-Hill Book Co., New York (1987) p. 669.

Table 1: Effect of the absolute permeability on the gas production

Absolute permeability, md	***Loss in Cumulative Gas Production, %***
0.1 md	32
1 md	20
10 md	5

Table 2: Effect of the Water and Gas Exponents of the Modified Brooks-Corey Relative Permeability Functions

Water and Gas Exponents	***Loss in Cumulative Gas Production, %***
nw=2 ng={2, 4, 6}	{5. 7. 9}
nw=4 ng={2, 4, 6}	{11, 20, 26}
nw=6 ng={2, 4, 6}	{14, 27, 27}

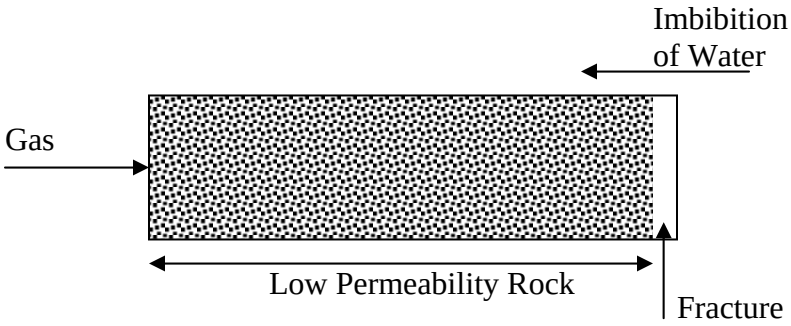

Figure 1. Rock-fracture system for 1-dimensional model.

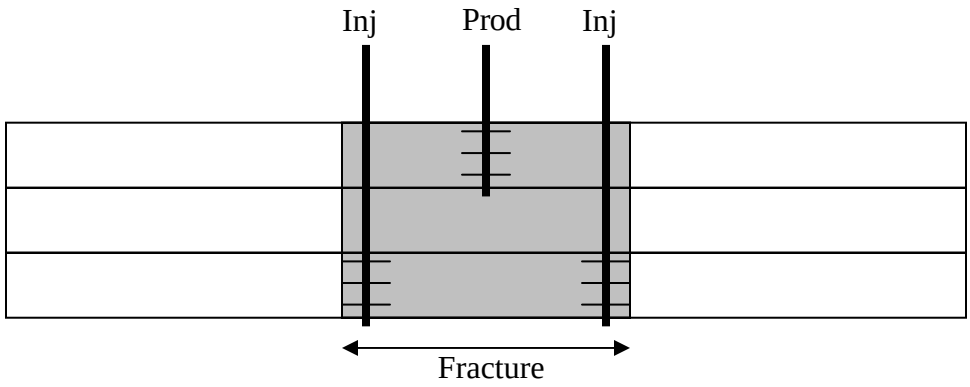

Figure 2. Location of the injectors and producer in fracture of the Cartesian model.

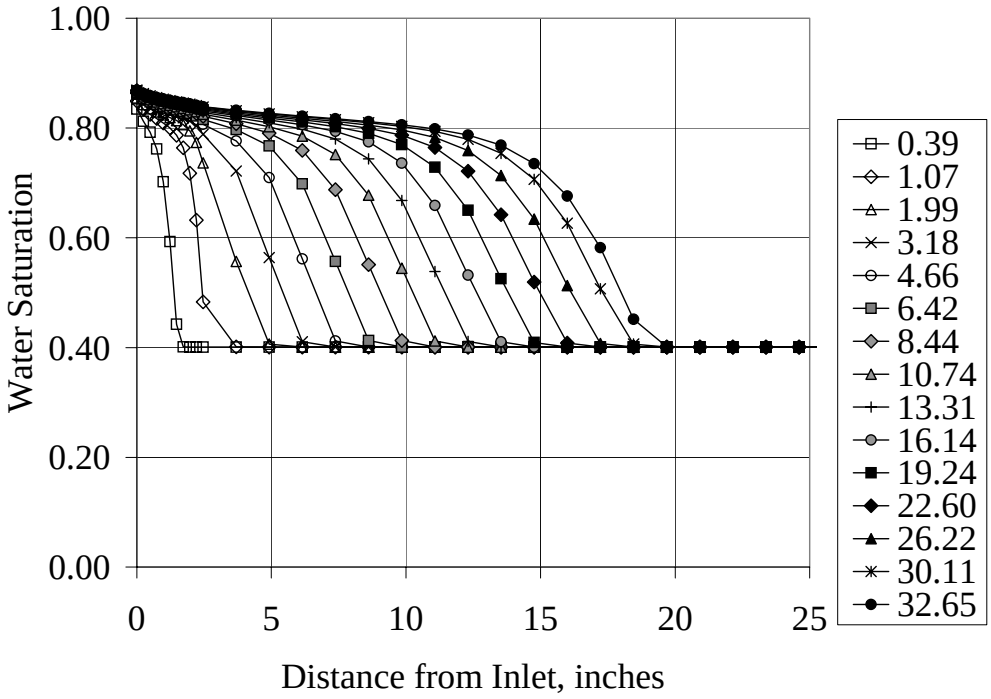

Figure 3. Water invasion during hydraulic fracturing: k = 0.010 md; k_{rwmax} = 0.1, k_{rgmax} = 0.8, nw = 4, ng = 2; P_{ct} = 100 psi, P_{cs} = 1500 psi; S_{wi} = 0.4, S_{gc} = 0.1. The legend pairs elapsed time in days with symbols of the figure.

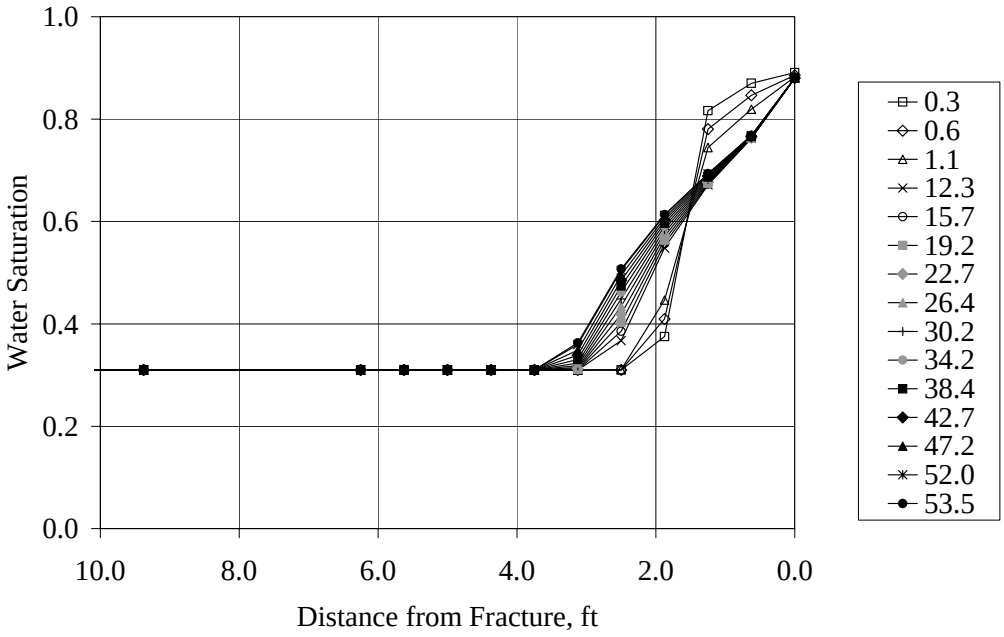

Figure 4. Water invasion after hydraulic fracturing for Base Case: k = 0.010 md; k_{rwmax} = 0.1, k_{rgmax} = 0.8, nw = 4, ng = 2; P_{ct} = 100 psi, P_{cs} = 500 psi; S_{wi} = 0.3, S_{gc} = 0.1; Step Width = 1.25 ft; ΔP = 1000 psi. The legend pairs elapsed time in days with symbols of the figure.

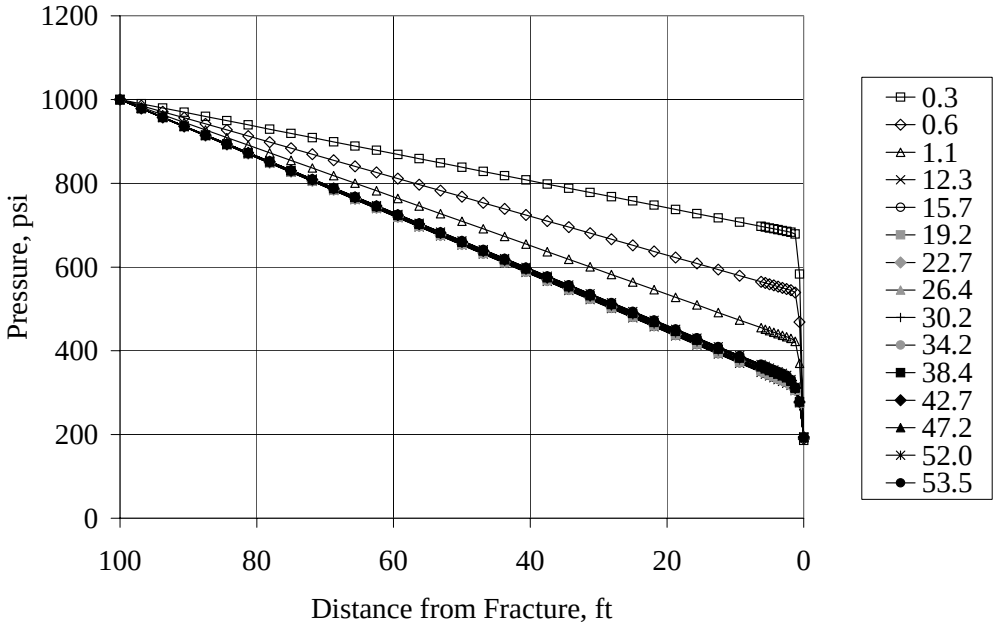

Figure 5. Pressure profiles after hydraulic fracturing (Base Case). The legend pairs elapsed time in days with symbols of the figure.

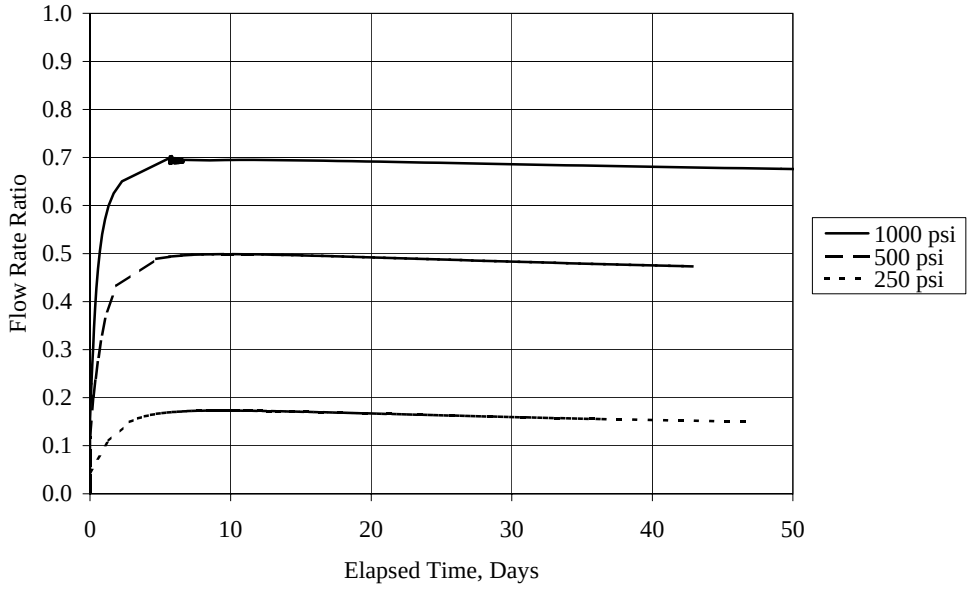

Figure 6. Effect of pressure drop on gas flow-rate ratio after hydraulic fracturing.

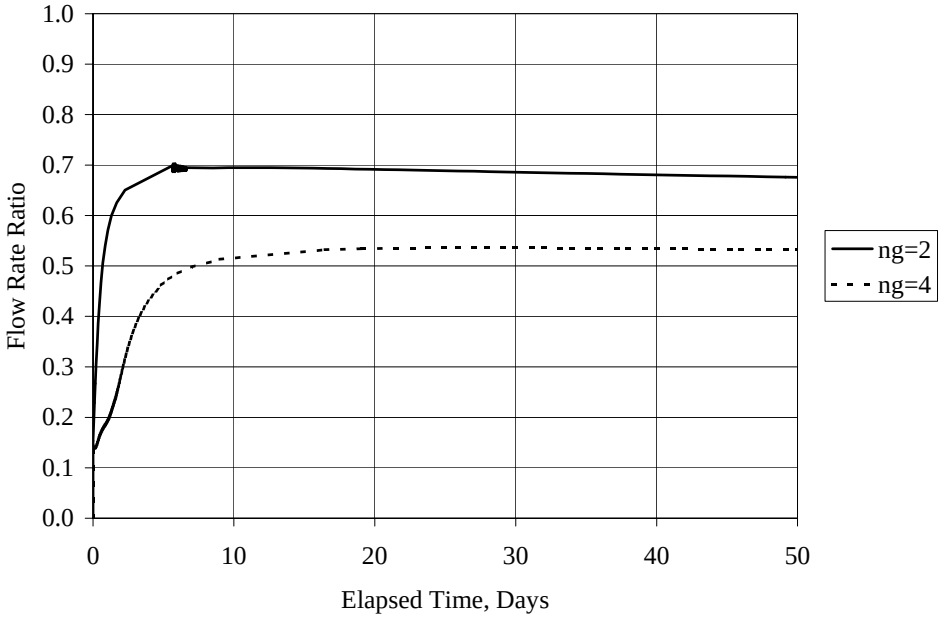

Figure 7. Effect of gas exponent ng on gas flow-rate ratio after hydraulic fracturing.

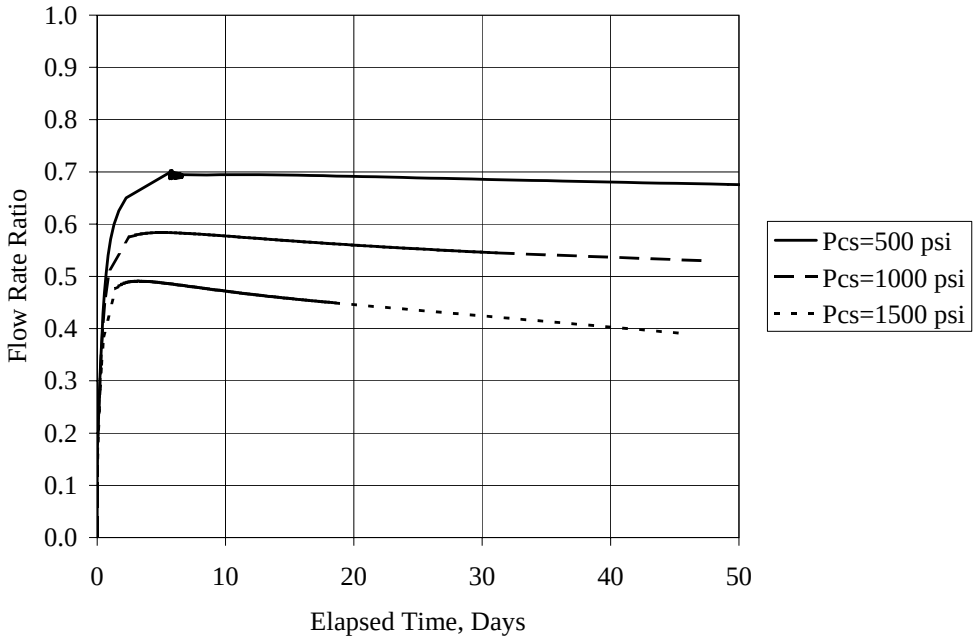

Figure 8. Effect of P_{cs} on gas flow-rate ratio after hydraulic fracturing.

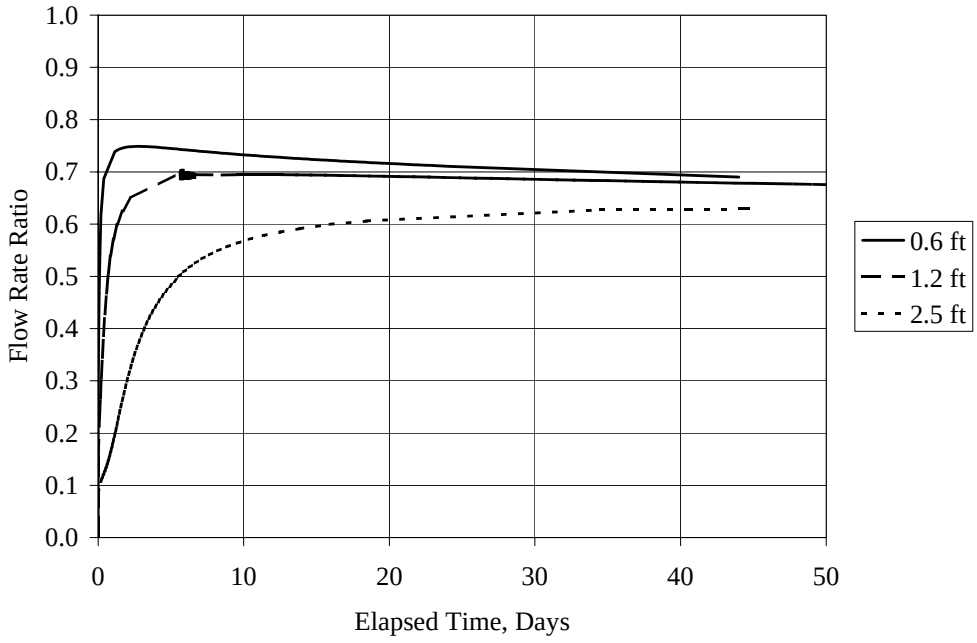

Figure 9. Effect of step width on gas flow-rate ratio after hydraulic fracturing.